LANGMUIR

Article

pubs.acs.org/Langmuir

Kinetic Control of Graphene Localization in Co-continuous Polymer Blends via Melt Compounding

Lian Bai, Radhika Sharma, Xiang Cheng,* and Christopher W. Macosko*

Department of Chemical Engineering and Materials Science, University of Minnesota, 421 Washington Ave. SE, Minneapolis, Minnesota 55455, United States

Supporting Information

ABSTRACT: Selective localization of graphene in co-continuous polymer blends is an attractive method for preparing conductive polymer composites. Localization of graphene at the interface between the two polymer phases produces good conductivity at ultra-low concentrations. Although graphene localization is ultimately dependent on thermodynamic factors such as the surface energy of graphene and the two polymer components, kinetics also strongly affects the migration and localization of graphene in polymer blends during melt compounding. However, few studies have systemically investigated the important role of kinetics on graphene localization. Here, we introduced graphene nanoplatelets (GNPs) in polylactic acid (PLA)/polystyrene (PS) co-continuous polymer blends. Although GNPs in thermal equilibrium prefer the PS phase, we were able to kinetically trap GNPs at the interface of polymer blends via control of melt-compounding sequences, mixing times and shear rates. Utilizing morphological, rheological, and electrical measurements, we verified graphene localization and the suppression of coarsening in co-continuous polymer blends during annealing. When GNPs were premixed with the thermodynamically less-favorable PLA phase before mixing with the PS phase, GNPs can be kinetically trapped at the interface during melt compounding. Moreover, we show that a shorter melt-compounding time gives rise to a higher GNP interfacial coverage and a more effective morphology stabilization effect. Blends with as low as 0.5 wt % GNPs with only 30 s of melt compounding have a room-temperature conductivity of $\sim 10^{-6}$ S/cm, which is larger than blends with longer melt-compounding times and potentially useful for antistatic materials. The in-depth study on the kinetics of graphene localization in our work provides a general guideline for the kinetic control of the localization of platelike nanofillers in polymer blends. Our study also demonstrates a facile method for manufacturing conductive polymer blends with low percolation thresholds.

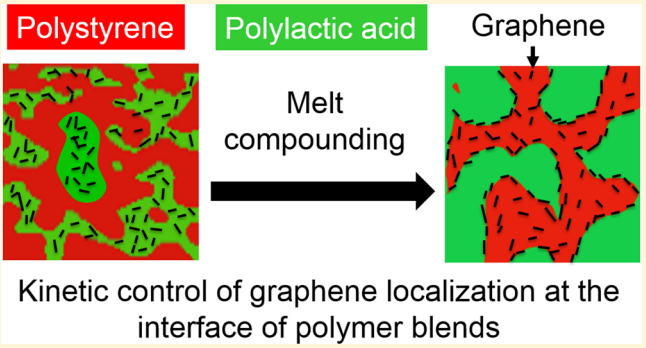

1. INTRODUCTION

Thanks to its two-dimensional structure, high aspect ratio, and superior electrical properties, graphene has attracted great attention for its application in electronics.[1,2] The addition of graphene to a polymer is an effective method for preparing conductive polymer composites (CPCs).[2,3] Selectively localizing graphene in one phase of co-continuous polymer blends[3,4] can effectively reduce the percolation thresholds by forming a double percolated structure.[5] To achieve even lower percolation thresholds, graphene can be selectively localized at the interface of co-continuous polymer blends.[6,7] In our previous work,[7] thermally reduced graphene oxide (r-GO) was localized at the interface of polystyrene (PS)/polylactic acid (PLA) co-continuous blends, resulting in a percolation threshold as low as 0.05 wt %.

To achieve good graphene dispersion, solution blending has been widely used. Mao and co-workers[4] dissolved poly(methyl methacrylate) (PMMA), PS and octadecylamine-functionalized graphene in tetrahydrofuran. Upon drying, the composites formed a co-continuous blend, where the modified graphene was all in the PS phase. Qi and co-workers[3] selectively localized graphene in the PS matrix of PS/PLA blends, using dimethylformamide (DMF). Tan and co-workers[6] grafted graphene with poly(styrene-*co*-methyl methacrylate) copolymer and dissolved grafted graphene, PS, and PMMA in DMF for preparing PMMA/PS co-continuous blends. In these solvent blending studies, the localization of graphene is dominated by thermodynamic factors, i.e., the surface energy of graphene and the two polymer components.[7,8] Similar to other conductive nanofillers such as carbon blacks[9,10] and carbon nanotubes,[11,12] graphene prefers to selectively remain in the polymer phase or at the interface of the two polymer phases, which minimizes the free energy of the entire system.

Special Issue: Early Career Authors in Fundamental Colloid and Interface Science

Received: August 30, 2017
Revised: October 9, 2017
Published: October 16, 2017

DOI: 10.1021/acs.langmuir.7b03085
Langmuir 2018, 34, 1073−1083

Compared with solution blending, melt compounding is a more cost-effective method to manufacture polymer blends.[13] Many efforts have been made to incorporate graphene into polymer blends using melt compounding. Shen and co-workers[14] have introduced chemically reduced graphene oxide at the interface of PLA/ethylene−vinyl acetate (EVA) co-continuous blends via melt compounding EVA with a PLA/r-GO master batch. Tu and co-workers[8] selectively localized graphene in the polyethylene (PE) phase of PE/polypropylene (PP) blends, using a twin screw extruder. In our previous work,[7] we localized thermally reduced graphene oxide (r-GO) at the interface of PLA/PS co-continuous polymer blends by melt-compounding PS with a PLA/r-GO master batch. When conductive nanofillers are melt-compounded into polymer blends, kinetic parameters such as compounding sequence,[7,8,14] melt viscosity of polymer components,[8,15,16] melt-compounding time,[9,17−19] and shear rate[13,20] significantly affect the migration and localization of graphene. Although these kinetic factors have been discussed in the literature related to carbon black[9,15,17,18] and carbon nanotubes,[13,16,19,20] to the best of our knowledge, no work has been published that has systemically studied the kinetic effect on the localization of platelike nanofillers, such as graphene, in polymer blends. Understanding and controlling graphene localization via kinetics during melt compounding is important for future applications of graphene-based conductive polymer composites, since the kinetic control certainly provides a more facile method for preparing conductive polymer composites.[8,10,21,22]

In this study, we incorporated graphene nanoplatelets into PLA/PS co-continuous blends by melt-compounding PS with a PLA/graphene master batch. With proper control of the melt-compounding sequence, shear rate, and mixing time, we were able to localize a large amount of graphene at the blend interface, which facilitates the stabilization of co-continuous morphology of the polymer blends and reduces the concentration needed for electrical percolation. The effect of melt-compounding sequence and time on the migration and localization of graphene were further studied through rheological and electrical measurements of the blends during annealing. We also investigated the change of the characteristic domain sizes of the co-continuous morphology, which provides a quantitative measurement of not only the structural change of the blends during annealing, but also the interfacial graphene coverage with different melt-compounding times. We found that a shorter melt-compounding time gives rise to higher interfacial graphene coverage and a more effective morphology stabilization effect during annealing.

2. EXPERIMENTAL SECTION

2.1. Materials. Polylactic acid (PLA, Ingeo Biopolymer 2003D, $T_m \approx 147$ °C, $\rho_{melt} = 1.12$ g/cm^3 at 180 °C) and polystyrene (PS, STYRON 666D, $T_g \approx 96$ °C, $\rho_{melt} = 0.98$ g/cm^3 at 180 °C) were obtained from NatureWorks LLC and Trinseo, respectively. The number-average molecular weights (M_n) of PLA and PS are 126 000 and 104 000, respectively. The polydispersity index (PDI) of PLA and PS are 1.87 and 2.50, respectively. The rheological properties of PLA and PS have been reported in our previous study.[7] While PS was used as received, PLA was dried further, under vacuum at 40 °C, overnight, before use. Graphene nanoplatelets (GNPs, N002-PDR, $\rho \approx 2.2$ g/cm^3) were purchased from Angstron Materials. According to the manufacturer, the average lateral dimension of the nanoplatelets is ≤10.0 μm and the thickness is ∼1.0−1.2 nm. The details about the characterization of GNPs thickness and lateral dimensions are provided in the Supporting Information.

2.2. Conductive Polymer Composites Preparation. *2.2.1. Master Batch Preparation.* PLA was first dissolved in *N*,*N*-dimethylformamide (DMF) at the concentration of ∼0.25 g/mL at 80 °C with stirring. The desired amount of GNPs was also dispersed in DMF at a concentration of ∼8.3 mg/mL, followed by exfoliation in a 100 W ultrasonic bath for 2 h. This suspension of GNPs in DMF was added into the PLA/DMF solution. After mechanically stirring the mixture for 2 h, we added the mixture dropwise into a large volume of vigorously stirred methanol to precipitate a PLA/GNPs master batch. The master batch was filtered and dried in an air circulating oven at 80 °C for at least 5 h to remove residual methanol. Finally, the dried PLA/GNPs master batch was further dried under vacuum at 40 °C overnight. In order to test the thermodynamic compatibility of PS and GNPs and the effect of different compounding sequences, we also prepared PS/GNPs master batches by following a similar procedure.

2.2.2. Melt Compounding. All the blends were mixed using a conical twin-screw microcompounder (Xplore MC5) at 180 °C under a nitrogen protective environment. The PLA/GNPs master batch was first added into the microcompounder at 50 rpm within 1 min. PS was then added at the same shear rate within 5 s. Finally, the shear rate was increased to 200 rpm for 5 min of melt compounding. The product was extruded and quickly quenched in liquid nitrogen to preserve the blend morphology. The shear rate of 200 rpm was chosen based on our study of melt compounding at different shear rates (see the Supporting Information). We found that 200 rpm was most effective to exfoliate GNPs and facilitate GNPs migration in the polymer matrix.

In order to study the kinetics of GNPs transfer during melt compounding, we prepared composites with different melt-compounding times. For all of the composites, we fixed the ratio of PLA/GNPs master batch and PS at 51.2/48.8 (weight ratio). In this paper, we use the notation, (PLA/GNPs)/PS_*x* wt %, to denote composites with *x* wt % GNPs premixed with PLA phase and then compounded with PS. Similarly, (PS/graphene)/PLA_*x* wt % is used to present composites with *x* wt % GNPs premixed with PS before compounding with PLA.

2.2.3. Annealing. A small piece (0.1−0.5 g) of each blend was placed between two sheets of fluoropolymer-coated fabric in a steel mold. The sample was then annealed at 180 °C for 10, 30, or 60 min in a Wabash hydraulic press under a pressure of ∼1.59 MPa. After annealing, the sample was cooled to room temperature in a water-cooled press for further analysis.

2.3. Sample Characterization. *2.3.1. Scanning Electron Microscopy (SEM).* The characteristic domain size was studied using scanning electron microscopy (SEM) (JEOL, Model 6500). Polymer blends after different annealing times were microtomed at room temperature with a glass knife. In order to image the interfaces between PLA and PS, microtomed samples were immersed in cyclohexane at 50 °C overnight to extract the PS phase, and then sputter-coated with 50 Å of platinum. The PLA porous sample after PS extraction was imaged at an accelerating voltage of 5 kV. We analyzed the resulting images using ImageJ by manually tracing the PLA/PS interface. The total length of the interface (L_{int}) in a specific SEM image was then measured. The characteristic domain size (ξ) can be determined as

$$\xi = \frac{A_{SEM}}{L_{int}} \quad (1)$$

where A_{SEM} is the total area of the SEM image. The characteristic domain size was obtained by averaging at least three different SEM images at the same annealing time. A similar calculation of the characteristic domain size has also been used in our previous study for bijels.[23]

2.3.2. Transmission Electron Microscopy (TEM). The localization of GNPs was studied by TEM (FEI Tecnai T12). Polymer blends after different annealing times were microtomed (∼50 nm thick) with a diamond knife at room temperature. The ultrathin sections were carefully transferred via an eyelash onto copper grids. The location of GNPs within the blends was then observed at an acceleration voltage of 120 kV. With the radiation-induced phase contrast,[24] the samples can be imaged with no further staining. Specifically, the electron

DOI: 10.1021/acs.langmuir.7b03085
Langmuir 2018, 34, 1073−1083

irradiation results in some degree of chain scission and mass loss of PLA, whereas PS, as one of the most radiation stable polymers, shows no loss of material under TEM.[24] Therefore, the phase contrast from the difference in mass/thickness makes the PLA phase the brighter regions and the PS phase the darker regions in a typical TEM image. GNPs were evident as thin black lines under TEM, which is due to the much larger electron density in the graphene structure.

2.3.3. Rheological and Dielectric Conductivity Measurements. Viscoelastic and dielectric spectra of samples were obtained simultaneously using a TA Instruments ARES rheometer with a TA Instruments Dielectric Thermal Analysis Accessory (DETA). An Agilent 4980A LCR bridge was attached on the 25 mm parallel plate of the rotational rheometer to apply AC voltages and measure the resulting current. During a rheology time sweep, the complex capacitance of samples (C^*) was monitored under a root-mean-square (rms) potential of 1 V with an AC frequency (ω_{AC}) between 20 Hz and 2 MHz. In order to compare with the annealing process in the hot press, the time sweeps were performed at 180 °C for 1 h with 1.0% strain and a rotational frequency of 1.0 rad/s. The relationship between the complex permittivity (ε^*) and the complex electrical conductivity (σ^*) can be calculated as

$$\varepsilon^* = \varepsilon' - i\varepsilon'' = \frac{C^* d}{\varepsilon_0 A} \tag{2}$$

$$\sigma^* = \sigma' + i\sigma'' = i\omega_{AC}\varepsilon_0\varepsilon^* = \omega_{AC}\varepsilon_0\varepsilon'' + i\omega_{AC}\varepsilon_0\varepsilon' \tag{3}$$

where ε_0 is the permittivity of a vacuum, A the area of the parallel plates, and d the separation of the parallel plates. The imaginary part of the complex permittivity (ε'') gives the real part of the complex conductivity (σ'), which represents the electrical loss of polymer composites due to free electron conduction. The plots reported in this study only show the real part of conductivity at an AC frequency of 20 Hz, because the dielectric conductivity at low AC frequency is independent of frequency and can be treated as the DC conductivity tested at 180 °C.[7,25] The change of dielectric conductivity as a function of AC frequency for (PLA/GNPs)/PS_0.5 wt % at different melt-compounding times after 60 min of annealing are shown in Figure S4 in the Supporting Information. The method used to test room-temperature DC conductivity directly on solid samples was reported in detail in the Supporting Information.

3. RESULTS AND DISCUSSION

3.1. Nanofiller Localization and Coarsening Suppression. The localization of nanofillers in the polymer blends can be qualitatively predicted by calculating wetting coefficients of GNPs.[23,26] Relevant to the current study, the wetting coefficient (ω) of GNPs in the PS/PLA blend is defined as

$$\omega = \cos\theta = \frac{\gamma_{GNPs/PLA} - \gamma_{GNPs/PS}}{\gamma_{PLA/PS}} \tag{4}$$

where θ is the three-phase contact angle of GNPs at the interface, and $\gamma_{GNPs/PLA}$, $\gamma_{GNPs/PS}$, and $\gamma_{PLA/PS}$ are the interfacial energies (or interfacial tensions) between GNPs and PLA, GNPs and PS, and PLA and PS, respectively. Because of the difficulties in experimentally measuring the interfacial energy between GNPs and polymers, all of these interfacial energies were theoretically derived, according to the Owens−Wendt equation,[27,28] using the harmonic mean of dispersive and polar part of surface energies. For example, $\gamma_{PLA/PS}$ can be calculated as

$$\gamma_{PLA/PS} = \gamma_{PLA} + \gamma_{PS} - 2\sqrt{\gamma_{PLA}^d \gamma_{PS}^d} - 2\sqrt{\gamma_{PLA}^p \gamma_{PS}^p} \tag{5}$$

where γ^d and γ^p are the dispersive component and the polar component of the surface energy of the components, respectively, at a processing temperature of 180 °C.

Based on eq 4, GNPs thermodynamically prefer to locate at the interface between PLA and PS when $-1 < \omega < 1$. When $\omega < -1$, GNPs locate in the PLA phase, whereas GNPs remain in the PS phase when $\omega > 1$. From the calculation shown in the Supporting Information, $\gamma_{GNPs/PLA}$ = 8.71 mJ/m^2, $\gamma_{GNPs/PS}$ = 2.21 mJ/m^2, and $\gamma_{PLA/PS}$ = 2.39 mJ/m^2. Therefore, the calculated wetting coefficient is 2.73, which suggests that, during melt compounding, GNPs would transfer completely from the premixed PLA phase (which is the thermodynamically less-favorable phase) to the PS phase.

Figure 1 shows TEM images of the (PLA/GNPs)/PS blends of 0.5 and 2.0 wt % GNPs without any annealing. As highlighted by the yellow arrows in Figure 1, some of the GNPs were located in the PS phase after 5 min of melt compounding at 180 °C, and very few of the GNPs can be found in the premixed PLA phase. The preference of GNPs for the PS phase is consistent with our wetting coefficient calculation shown above. Similar selective localization of graphene in PLA/PS blends via solution blending was also observed by Mao et al.[4] More interestingly, a significant fraction of GNPs can be found at the interface between the PLA phase and the PS phase, as highlighted by the white arrows in Figure 1. These interfacial GNPs were kinetically trapped at the interface during melt compounding and failed to achieve the thermodynamic equilibrium. The effect became more obvious at longer annealing times, when the domains of the co-continuous structure were larger. Figure 2 shows TEM images of the (PLA/GNPs)/PS blends of 0.5 and 2.0 wt % GNPs after 60 min annealing at 180 °C. Because of the high viscosity of PS and the relatively large lateral dimensions of GNPs (average area of ~1.25 μm^2), the migration of interfacial GNPs into the PS phase during annealing in the direction perpendicular to the interface was very slow. Therefore, the interfacial GNPs still remained at the interface, even after 60 min of annealing, as highlighted by the white arrows in Figure 2.

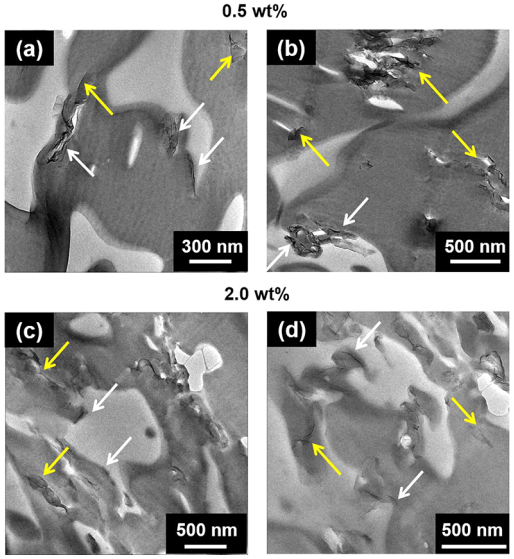

Figure 1. TEM images of (PLA/GNPs)/PS blends after 5 min of mixing without any annealing: (a, b) 0.5 wt % GNPs and (c, d) 2.0 wt % GNPs. The darker phase is PS and the lighter phase is PLA. The black lines are GNPs. The interfacial GNPs are highlighted by the white arrows, while GNPs in the PS phase are highlighted by the yellow arrows.

DOI: 10.1021/acs.langmuir.7b03085
Langmuir 2018, 34, 1073−1083

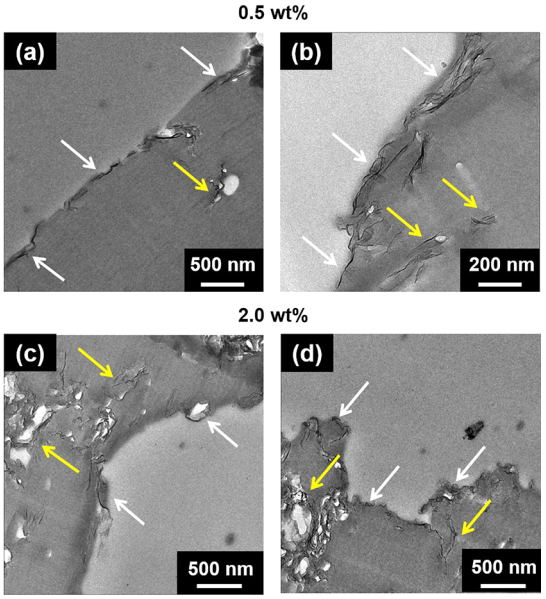

Figure 2. TEM images of (PLA/GNPs)/PS blends after 5 min of mixing and 60 min of annealing at 180 °C: (a, b) 0.5 wt % GNPs and (c, d) 2.0 wt % GNPs. The interfacial GNPs are highlighted by the white arrows, while GNPs in the PS phase are highlighted by the yellow arrows.

The effect of coarsening suppression due to the presence of GNPs in the PLA/PS co-continuous polymer blends are compared in Figure 3. Figure 3a shows the characteristic domain size (ξ) of the PLA/PS blends with different loadings of GNPs, as a function of annealing time at 180 °C. The neat blend exhibits an increase of the domain size from ~2 μm up to ~77 μm within 60 min of annealing. When 0.5 wt % GNPs were premixed with PLA and then melt-compounded with PS, the domain size gradually increases from ~2 μm to ~15 μm after 30 min of annealing. The characteristic domain increases much slower after 30 min of annealing and seems to gradually approach a plateau of ~16 μm after 60 min of annealing. When the GNPs loading is increased to 2.0 wt %, the characteristic domain size slightly increases during the first 10 min of annealing and then approaches a plateau of ~2.5 μm after 60 min of annealing.

The coarsening suppression of (PLA/GNPs)/PS blends is due to a synergistic effect from both the GNPs in the PS phase and those trapped at the interface. First, the GNPs located in the PS phase (see Figures 1 and 2) increase the viscosity of the PS phase and slow the coarsening of the PLA/PS blend. A quantitative measurement of the viscosity increase of the PS phase due to the presence of GNPs was shown in the Supporting Information. More importantly, because of the reduction of interfacial area during coarsening, the GNPs located at the interface form contacts with each other and gradually establish an interfacial GNPs network. The formation of a GNP network at the interface prevents further shrinkage of interfacial area and finally arrests the domain coarsening. As the interfacial area shrank during annealing, the average planar density of the interfacial GNPs became higher for blends after 60 min of annealing than blends without annealing, which is an effect that can be qualitatively observed by comparing 0.5 wt % blends in Figures 1 and 2. Note that the interfacial GNPs in our study merely formed a sparse network at the PLA/PS interface, instead of fully covering and jamming at the interface as r-GO in PLA/PS co-continuous blends.[7]

The change of characteristic domain sizes during annealing of PLA/PS blends with r-GO jammed at the interface (data taken from ref 6) is also shown in Figure 3. When the filler loading is 0.5 wt % (0.28 vol % for r-GO), r-GO is more effective to suppress the coarsening and stabilize the co-continuous morphology than GNPs, since r-GO prefers to locate at the interface thermodynamically.[7] Except for a small amount of r-GO aggregates that remained in the premixed PLA matrix, most of r-GO was located at the interface from TEM (see Figure 2 in ref 6). In comparison, GNPs prefer to remain in the PS phase thermodynamically. While some GNPs were kinetically trapped at the interface, others migrate to the PS phase during melt compounding. Therefore, at the same weight fraction, the amount of interfacial GNPs is smaller than that of interfacial r-GO. Hence, the blends with 0.5 wt % r-GO have more interfacial r-GO to effectively arrest the coarsening, which

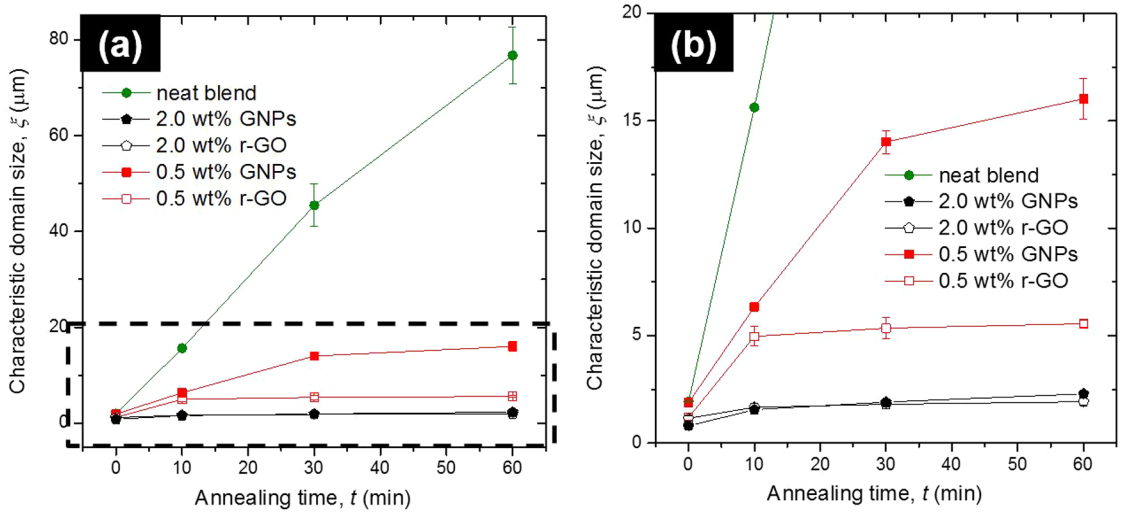

Figure 3. (a) Characteristic domain sizes (ξ), as a function of annealing time at 180 °C, for PLA/PS neat blend, (PLA/r-GO)/PS blends[7] and (PLA/GNPs)/PS blends of different filler contents. (b) Enlarged view showing the details of the region highlighted by a dashed border at the bottom of panel (a).

DOI: 10.1021/acs.langmuir.7b03085
Langmuir 2018, 34, 1073−1083

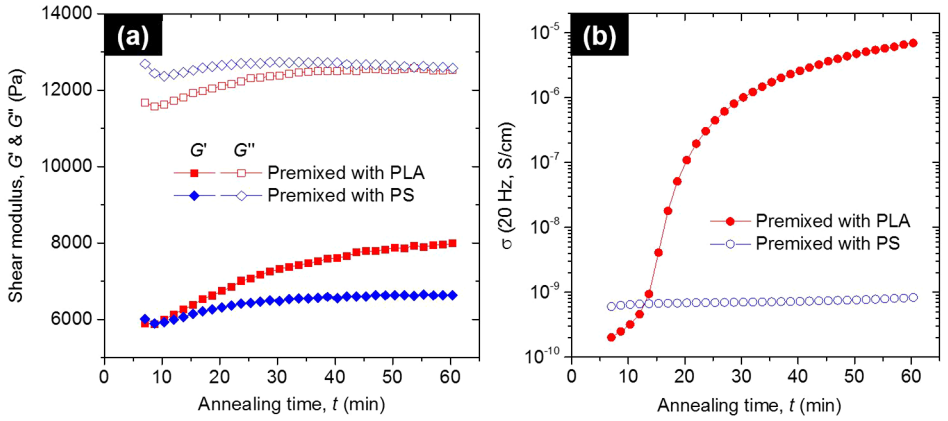

Figure 4. (a) Shear modulus and (b) dielectric conductivity, each as a function of annealing time at 180 °C for PLA/PS blends with 0.5 wt % GNPs using two different compounding sequences: GNPs premixed with PLA and GNPs premixed with PS. The data were measured at a rotation frequency of 1.0 rad/s and a strain of 1.0%.

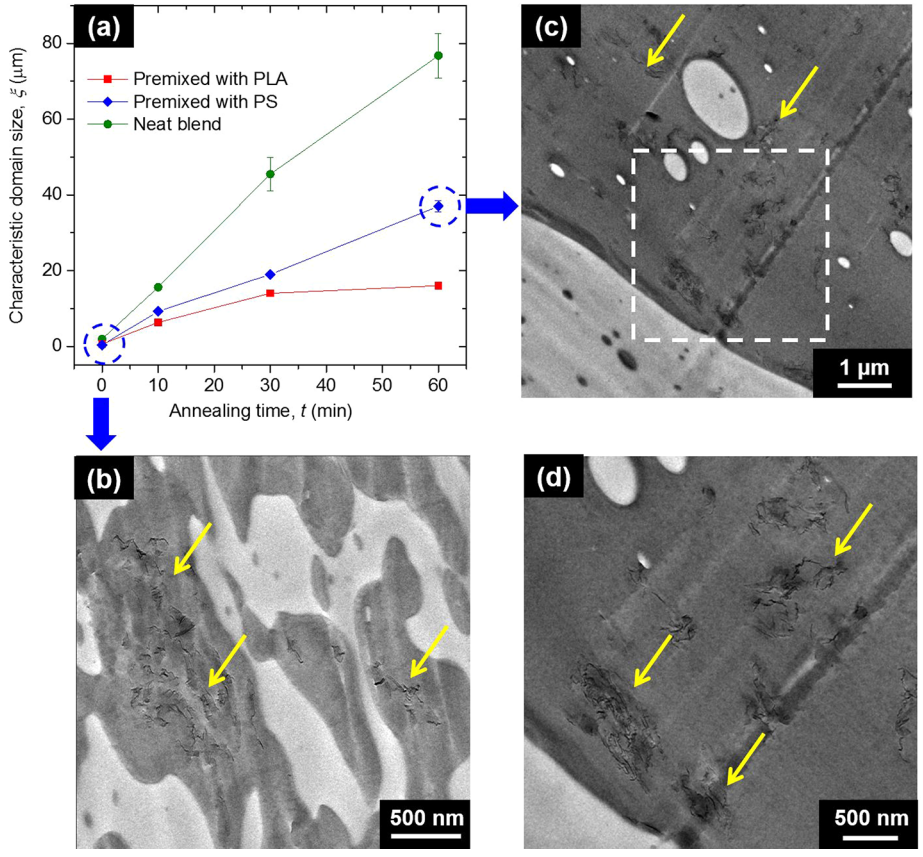

Figure 5. (a) Characteristic domain size (ξ), as a function of annealing time at 180 °C for PLA/PS neat blends, (PLA/GNPs)/PS_0.5 wt % blends, and (PS/GNPs)/PLA_0.5 wt % blends. (b, c) TEM micrographs of the (PS/GNPs)/PLA_0.5 wt % blends: without annealing (panel (b)) and after 60 min of annealing (panels (c) and (d)). The darker phase is PS, and the lighter phase is PLA. The black lines are GNPs. GNPs in PS are highlighted by the yellow arrows. The magnified image depicted in panel (d) shows the selected region highlighted by the white dashed border in panel (c).

results in smaller domains. This comparison between r-GO and GNPs suggests that interfacial GNPs are more effective to suppress the coarsening and stabilize the co-continuous morphology than the GNPs in the PS phase. When the fillers loading is further increased to 2.0 wt % (1.12 vol % for r-GO), the coarsening suppression effect of r-GO and GNPs are almost the same. This is due to the dramatically increased viscosity of the GNPs located in the PS phase (see Figure S5(a) in the Supporting Information), which could also effectively slow the coarsening and stabilize the co-continuous morphology. Similar phenomena have been observed in other nanofillers selectively located and percolated in a single polymer phase of polymer blends.[4,9,10,29]

3.2. Effect of Different Melt-Compounding Sequences. As shown in Figures 1 and 2, the localization of a significant amount of GNPs in the PLA/PS interface does not match the wetting coefficient calculation, which predicts the localization of all GNPs in the PS. The wetting coefficient

DOI: 10.1021/acs.langmuir.7b03085
Langmuir 2018, 34, 1073−1083

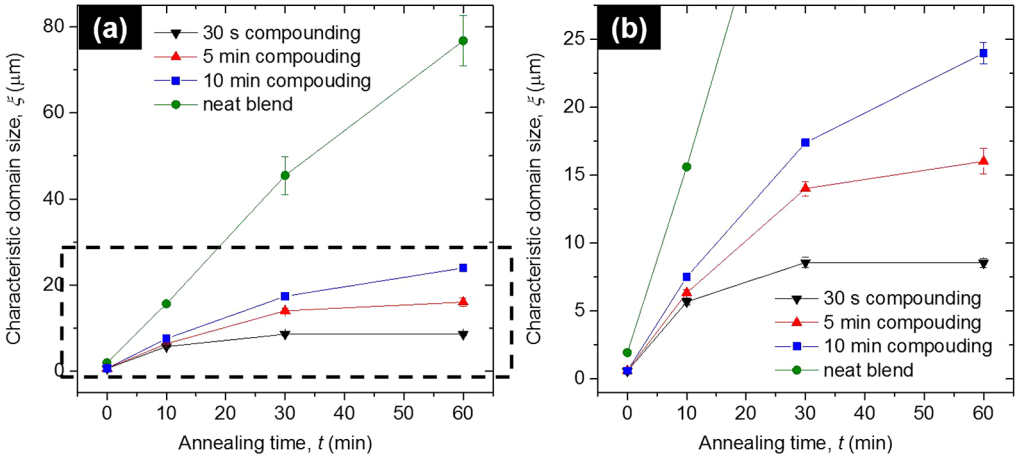

Figure 6. (a) Characteristic domain size (ξ), as a function of annealing time at 180 °C, for PLA/PS neat blends and (PLA/GNPs)/PS_0.5 wt % blends with melt-compounding times of 30 s, 5 min, and 10 min. (b) Magnified image showing the detail of the selected region highlighted by the black dashed border in panel (a).

calculation is purely based on the thermodynamic interactions of GNPs with polymeric phases. Kinetic parameters, such as the melt-compounding sequence of polymeric components[7,30,22,31] and melt-compounding time,[9,13,17−19] also affect the distribution of nanofillers in the polymer blends. In the following, we chose PLA/PS blends with 0.5 wt % GNPs as our reference to investigate the effects of the kinetic factors on the localization and migration of GNPs in the blend. Both the rheological and electrical properties of the conductive-fillers-filled polymer blends are sensitive to the localization and distribution of conductive fillers in the blends.[7,10,21] We used a dielectric setup on the parallel plate rheometer to simultaneously record the rheology and conductivity of the blends during annealing at 180 °C. All dielectric conductivities plotted in this study were measured at 20 Hz. Because a finite time was required to prepare the sample under hot pressing and load the sample into the setup, the first data point represents the shear modulus and conductivity of the blend after 7 min of annealing.

Figure 4 records the variation of the shear modulus and dielectric conductivity with annealing times for PLA/PS blends with 0.5 wt % GNPs using different compounding sequences. For the (PLA/GNPs)/PS_0.5 wt % blend, both the storage modulus (G') and the dielectric conductivity (σ) first sharply increase after ∼10 min of annealing and then change to a more gradual increase after ∼30 min of annealing. The increase in G' and σ is mainly due to the formation of a network by the interfacial GNPs during the coarsening. The network provides a mechanical scaffold, as well as a path for electrons to pass through the sample. Note that the dielectric conductivity of (PLA/GNPs)/PS_0.5 wt % blend is an order of magnitude larger than that of (PLA/r-GO)/PS_0.5 wt % (or 0.28 vol %) in our previous work.[7] This is due to the higher C/O ratio of GNPs than r-GO (see Table S1 in the Supporting Information), which leads to a higher conductivity of GNPs, compared with that of r-GO. More importantly, with a different compounding sequence for the (PS/GNPs)/PLA_0.5 wt % blend, G' clearly shows a less sharp increase. The plateau G' value of the (PS/GNPs)/PLA_0.5 wt % blend is obviously smaller than that of the (PLA/GNPs)/PS_0.5 wt % blend. More strikingly, σ of the (PS/GNPs)/PLA_0.5 wt % blend is more than 3 orders of magnitude smaller than the (PLA/GNPs)/PS_0.5 wt % blend after 60 min of annealing (see Figure 4b).

The different rheological and electrical properties arise from different coarsening behaviors and GNPs distributions in the (PLA/GNPs)/PS_0.5 wt % and (PS/GNPs)/PLA_0.5 wt % blends. As shown in Figure 5a, the characteristic domain size of the (PS/GNPs)/PLA_0.5 wt % blend does not reach the plateau after annealing, and the final value was almost twice of that of the (PLA/GNPs)/PS_0.5 wt %. The localization of GNPs in (PS/GNPs)/PLA_0.5 wt % blend was further observed under TEM. Without annealing, all GNPs appear to be located in the premixed PS phase after melt compounding (Figure 5b). After annealing for an additional 60 min at 180 °C, all GNPs still remain in the thermodynamically more favorable PS phase (Figure 5c and 5d), and very little of the interface is covered by GNPs. Thus, for the (PS/GNPs)/PLA_0.5 wt % blend, GNPs in the PS phase merely slow the coarsening, because of the effect of viscosity increase (see Figure S5(a)). Therefore, the comparison of G', σ, and domain size change during annealing between PLA/PS blends with 0.5 wt % GNPs in different compounding sequences indicates that the GNPs in the PS phase have limited contribution to the increase of G' and σ and the coarsening suppression in the (PLA/GNPs)/PS_0.5 wt % blend. For the (PLA/GNPs)/PS_0.5 wt % blend, the effective morphology stabilization is mainly due to the existence of interfacial GNPs and the formation of GNPs network along the interface. Similarly, the interfacial GNPs network dominates the increases in the storage modulus and the electric conductivity in the (PLA/GNPs)/PS_0.5 wt % blend.

3.3. Effect of Different Melt-Compounding Times. To investigate the effect of melt-compounding times on the migration and localization of GNPs in the PLA/PS co-continuous polymer blends, (PLA/GNPs)/PS_0.5 wt % blends with melt-compounding times of 30 s, 5 min, and 10 min were prepared. As shown in Figure 6, compared with the PLA/PS neat blend, the (PLA/GNPs)/PS_0.5 wt % blends with different melt-compounding times successfully suppress the coarsening but to different degrees. The coarsening of the 30 s compounded blend was effectively arrested, with a domain size plateauing at ∼8 μm after long annealing times. The coarsening of the 5 min compounded blend is also effectively suppressed,

DOI: 10.1021/acs.langmuir.7b03085
Langmuir 2018, 34, 1073−1083

but the characteristic domain size still slightly increases after 30 min of annealing and finally reaches ~16 μm at long annealing times. In comparison, the coarsening of the blend with 10 min of compounding was only partially suppressed, and the characteristic domain size continuously increased, although at a smaller rate than the neat blend. As discussed in Section 3.2, the interfacial GNPs dominates the coarsening suppression of the co-continuous morphology. Given the same GNPs loading, the effectiveness in morphology stabilization is mainly determined by the amount of GNPs that are trapped at the interface. Thus, the characteristic domain size can be used as an indicator to reflect the percentage of interfacial GNPs in the blend. The smaller characteristic domain size of (PLA/GNPs)/PS_0.5 wt % with 30 s of compounding suggests a higher percentage of GNPs located at the interface, which provides a more effective way to suppress coarsening.

The localization of GNPs in the (PLA/GNPs)/PS_0.5 wt % blends with melt-compounding times of 30 s and 10 min, with and without annealing, was further shown in TEM (Figure 7).

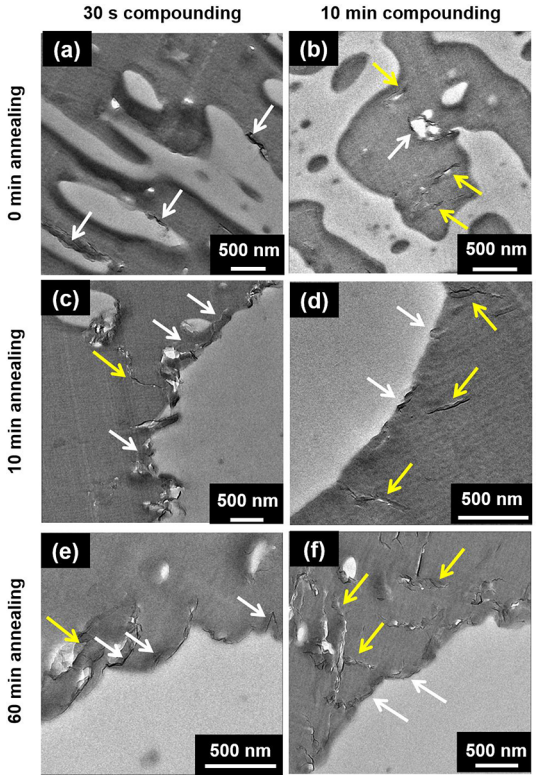

Figure 7. TEM images of (PLA/GNPs)/PS_0.5 wt % blends, for 30 s of compounding after (a) 0, (c) 10, and (e) 60 min of annealing; and for 10 min of compounding after (b) 0, (d) 10, and (f) 60 min of annealing. The interfacial GNPs are highlighted by the white arrows, while GNPs in PS phase are highlighted by the yellow arrows.

For as-prepared blends without any annealing, it is obvious that the blend that was compounded for 30 s has more GNPs located at the interface than the blend compounded for 10 min (see Figures 7a and 7b). As we have discussed above, the migration of interfacial GNPs to the PS phase during annealing should be negligible, because of the high melt viscosity of the polymer matrix and relatively large lateral dimension of GNPs. Based on this assumption, the coarsening during annealing only shrinks the interfacial area and changes the planar density of interfacial GNPs. The coarsening does not change the percentage of interfacial GNPs versus total GNPs loading in the blend. Therefore, even after 10 and 60 min of annealing, the 30 s compounded blend (Figures 7c and 7e) still has more interfacial GNPs than that of the 10 min compounded blend (Figures 7d and 7f). Indeed, the interfacial GNPs of the 30 s compounded blend already jam at the interface after 30 min of annealing, as suggested by the plateau of the domain size in Figure 6b.

The smaller amount of interfacial GNPs after longer melt compounding is mainly caused by the fluid flows during melt compounding. From the domain size (Figure 6) and TEM images (Figures 7a, 7c, and 7e), it is known that GNPs migrate from the premixed PLA phase to the interface within 30 s of compounding. As illustrated in the schematics (Figure 8), the repeated stretching and folding of the compounding flows in the microcompounder can encapsulate the interfacial GNPs into PS. Thus, a longer compounding time will lead to a more effective transfer of GNPs toward PS. The mechanism also predicts that GNPs in PS close to the interface are more likely to be perpendicular to the interface (see Figures 7b and 7d, as well as Figures S8(h) and S8(i) in the Supporting Information). The folding of interfaces occurs because of the low interfacial coverage of GNPs during melt compounding (Figure 7a for the 30 s compounded melt blend without any annealing).

In addition to the mechanism related to the folding of interfaces discussed above, the different migration rates of interfacial GNPs in different orientations during melt compounding also affect the amount of GNPs at the interface. The orientation of GNPs, with respect to the interface can be quantitatively measured by the three-phase contact angle θ, which is the angle between the interface and the lateral direction of GNPs (see Figure S6 in the Supporting Information). Note that, because of polar symmetry, $\theta \in [0, \pi/2]$. We further categorize the GNPs trapped at the interface into two groups: (1) parallel GNPs with $0 \leq \theta \leq \pi/18$ and (2) angular GNPs with $\pi/18 < \theta \leq \pi/2$. For the 30 s compounded blend, GNPs in both categories were observed at the interface (see Figures 7a, 7c, and 7e), while very few GNPs could be found in PS. The observation indicates that the melt-compounding time of 30 s is still not sufficient for GNPs migration to the PS phase. More TEM images of the 30 s compounded blend after 60 min of annealing can be found in the Supporting Information (Figure S7). Based on the TEM images of the 30 s compounded blend after 60 min of annealing, we measured the orientation of more than 220 GNPs at the interface (Figure 7e and Figure S6). We found that the ratio of interfacial GNPs in the parallel orientation, versus those in the angular orientation, is 0.84. If the orientation of the interfacial GNPs is completely random, the ratio should be much smaller at $\frac{\pi}{18}/\left(\frac{\pi}{2} - \frac{\pi}{18}\right) = 0.125$. The difference suggests that the flow during melt compounding and the interfacial attachment of GNPs result in a strong bias toward orientation parallel to the interfaces. More interestingly, when compared with the 10 min compounded blend, where we measured more than 160 GNPs at the interface (see Figure 7f, as well as Figure S7 in the Supporting Information), we found that GNPs of the angular orientation are more likely to migrate to PS under further melt compounding (Figures 7b, 7d, and 7f). Correspondingly, the ratio of parallel GNPs to angular GNPs increases to 2.0. Again, more TEM images of the 10 min compounded blend after 60 min of annealing can be found in Figure S8 in the Supporting Information. Such an orientation-

DOI: 10.1021/acs.langmuir.7b03085
Langmuir 2018, 34, 1073−1083

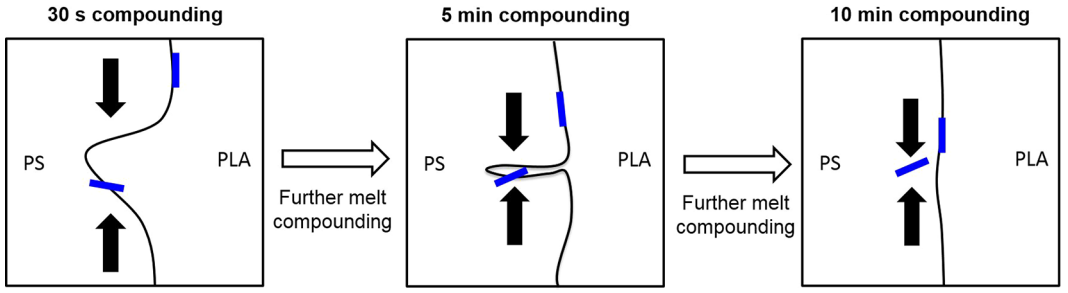

Figure 8. Schematics showing how the compounding flow during melt compounding pinches off and folds over the interface, and finally encapsulates interfacial GNPs into PS. GNPs are represented by blue lines, while the melt flow direction is highlighted by solid black arrows.

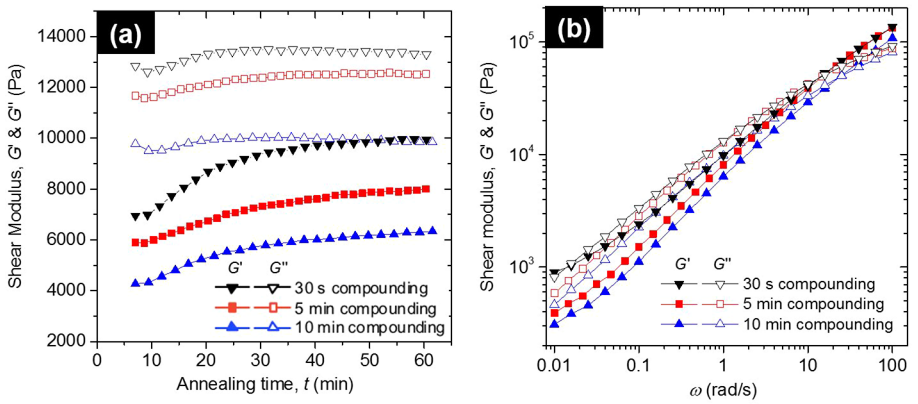

Figure 9. (a) Shear modulus, as a function of annealing time at 180 °C, for (PLA/GNPs)/PS_0.5 wt % blends with different melt-compounding times. The data were measured at a frequency of 1.0 rad/s and strain of 1.0%. (b) Shear modulus as a function of frequency after 60 min annealing at 180 °C of (PLA/GNPs)/PS_0.5 wt % blends with different melt-compounding times.

dependent GNP migration directly determines the interfacial coverage of GNPs at different compounding times. Therefore, both the orientation-dependent interfacial GNPs migration and interfacial GNPs encapsulation via interface folding contribute to the lower interfacial coverage of GNPs in the 10 min compounded blend, compared with the 30 s compounded blend.

The orientation-dependent migration of nanofillers can be understood as follows. Favis and co-workers[31] studied the migration of silica nanoparticles from the PLA/poly(butylene adipate-*co*-terephtahlate)(PBAT) blend interface to the thermodynamic favorable PBAT phase. They found that nanofiller migration from the interface to a polymer phase is a process of dynamic wetting of the solid phase of the particles by the liquid phase of the polymer. Therefore, the migration speed of nanofillers is equivalent to the displacement speed of the three-phase contact line (V), which can be estimated as[32,33]

$$V = \frac{F}{\xi L} \tag{6}$$

where F is the thermodynamic driving force to drag nanofillers from interface to the thermodynamic favorable phase during melt compounding.[34] The driving force decreases when approaching the equilibrium localization of nanofillers and finally vanishes when the equilibrium state is achieved. L is the three-phase contact line, and ξ is the friction coefficient. If we apply eq 6 to the GNPs in this study, L for GNPs in parallel orientation is the lateral dimension of GNPs: ∼1.47 μm (see Figure S2). However, L for GNPs in angular orientation is similar to the thickness of GNPs: ∼1.3 nm (see Figure S1). The friction parameter ξ is given by the viscosity of PS.[32] Since F and ξ are the same for the GNPs in different orientations, the migration speed of GNPs in the angular orientation should be more than 1000 times larger than that of GNPs in the parallel orientation. This explains why most GNPs in the angular orientation migrate into PS after 10 min of compounding, which gives rise to the smaller interfacial GNPs coverage, compared with that of the 30 s compounded blend. A similar phenomenon has also been observed by Göldel et al. in their study of the Slim-Fast Mechanism.[12] They found that nanofillers with high aspect ratios (e.g., carbon nanotubes) have faster migration speeds through blend interfaces than those with low aspect ratios (e.g. carbon blacks). The high migration speeds were observed only for high-aspect-ratio nanofillers in the angular orientation, while the nanofillers with the parallel orientation do not show enhanced migration speeds (see Figures 5c and 5d in ref 11).

In addition to the characteristic domain size and TEM images, the rheology and conductivity of (PLA/GNPs)/PS_0.5 wt % blends with different melt-compounding times also provide further insights on the migration and localization of GNPs in the blends. Figure 9a illustrates the change of the shear modulus. The increase of G' suggests the formation of GNPs network along the interface during coarsening. The larger G' of blends with shorter compounding time is mainly attributed to smaller domain size and, correspondingly, larger interfacial area. Figure 9b shows the rheology frequency sweeps after 60 min of annealing. In the low-ω region, the G' of blend with 30 s of compounding is even larger than G'' and shows a plateau with a smaller terminal slope than blends with 5 and 10 min of compounding. Both of these factors indicate the jamming of interfacial GNPs (Figure 7e). For blends with 5 and

DOI: 10.1021/acs.langmuir.7b03085
Langmuir 2018, 34, 1073−1083

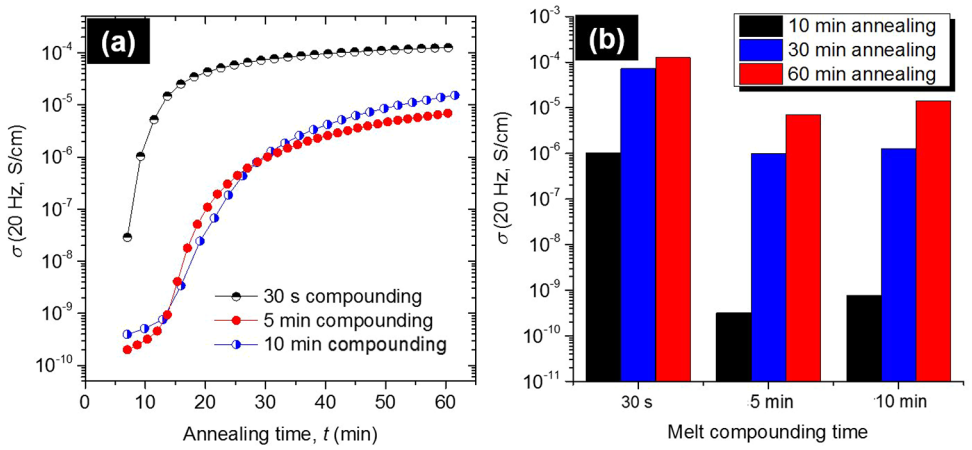

Figure 10. (a) Dielectric conductivity at ω_{AC} = 20 Hz, as a function of annealing time at 180 °C, for (PLA/GNPs)/PS_0.5 wt % blends with different melt-compounding times. The data were measured at a rotation frequency of 1.0 rad/s and a strain of 1.0%. (b) Column chart showing dielectric conductivity at ω_{AC} = 20 Hz for (PLA/GNPs)/PS_0.5 wt % blends with different melt-compounding times at different annealing times at 180 °C.

10 min of compounding, the GNPs network along the interface is loosely packed and still far from close-packed jamming (recall Figures 2a and 7f). Therefore, G' in the low-ω region is smaller than G'' and the terminal slope is larger than that of the 30 s compounded blend.

Figure 10a displays the dielectric conductivity of the (PLA/GNPs)/PS blends at 180 °C. For the blend with 30 s of melt compounding, the conductivity dramatically increases within the first 20 min of annealing and reaches a plateau conductivity value of ~10^{-4} S/cm. However, for blends with longer melt-compounding times (5 and 10 min), the conductivity is ~2 orders of magnitude smaller and exhibits much slower increases at the beginning and then, after 15 min of annealing, changes to a sharp increase, similar to the sample with 30 s of melt compounding, which finally slows and reaches a small conductivity at ~10^{-5} S/cm after long-term annealing. The sharp increase of conductivity in the conductivity vs nanofiller contents corresponds to the percolation threshold. Specifically, the formation of GNPs network along the interface contributes to the observed electrical percolation. For the 30 s compounded blend, the higher interfacial GNPs percentage makes the formation of GNPs network along the interface faster during annealing than blends with longer compounding times. The electrical percolation of the 30 s compounded blend occurs ~10 min earlier than that of blends with longer compounding times. This also explains why, after 10 min of annealing, the 30 s compounded blend has higher conductivity (by ~2 orders of magnitude) than that of the 5 and 10 min blends (Figure 10b). The conductivity plateau of the 30 s compounded blend after 30 min of annealing corresponds to the plateau of characteristic domain size in Figure 6b. The interfacial GNPs in this blend jam at the interface and result in high conductivity with a long plateau. However, for blends with compounding times of 5 and 10 min, the continuous conductivity increases after 30 min of annealing are related to the continuous coarsening in characteristic domain size (Figure 6b). The continuous rearrangement of the loosely packed GNPs network along the interface during coarsening gives rise to the slow increase in conductivity at long annealing times. Finally, after 60 min of annealing, because of the shrinkage of the interfacial area and the increase of interfacial GNPs density, the difference in conductivity among these three blends is significantly reduced (see Figure 10b). The higher conductivity of the blend with a compounding time of 30 s is attributed to the most densely packed interfacial GNPs. It is not clear why the conductivity of the blend with 10 min of melt compounding is almost the same with 5 min of melt compounding, whose interfacial GNPs percentage is actually larger. Lastly, it is worth noting that the conductivities shown in Figure 10 are dielectric conductivities measured at 180 °C, which is different from room-temperature DC conductivities. The room-temperature DC conductivity of (PLA/GNPs)/PS_0.5 wt % blends with 30 s, 5 min, and 10 min of compounding after 60 min of annealing are 1.3 × 10^{-6} S/cm, 1.6 × 10^{-7} S/cm (Figure S3 in the Supporting Information), and 6.4 × 10^{-7} S/cm, respectively. Even though these DC conductivities are relatively small, compared to the dielectric conductivities at 180 °C, blends with a conductivity of ~10^{-6} S/cm have potential applications as antistatic materials.[1] Our measurements on the DC conductivity of solid samples at room temperature can be found in the Supporting Information.

In summary, we found that 30 s of compounding is more effective than longer compounding times (5 and 10 min) to kinetically trap GNPs at the interface and, therefore, provides a better procedure for preparing co-continuous conductive polymer blends. We showed that the (PLA/GNPs)/PS_0.5 wt % blend with 30 s of compounding has a large interfacial GNPs coverage, a smaller plateau domain size, a higher storage modulus, and a larger conductivity. The study of the effect of melt compounding is of great importance in industrial applications. Limited by the length of screws and the time cost, it is more efficient to decrease the melt-compounding time in large-scale continuous twin screw extruders. The higher interfacial stability of GNPs via controlling the melt-compounding time facilitates the commercialization of the conductive polymer composites based on co-continuous polymer blends with interfacial GNPs. Note that our study demonstrates only the general principle. The specific compounding time of 30 s applies only in our system. This optimal compounding time varies, depending on the specific polymer blend and processing temperature chosen in different applications.

DOI: 10.1021/acs.langmuir.7b03085
Langmuir 2018, 34, 1073−1083

4. CONCLUSIONS

In this study, we have shown that graphene nanoplatelets (GNPs) can be kinetically trapped at the interface of co-continuous PLA/PS blends via a proper control of compounding sequences, melt-compounding times, and shear rates. Based on the prediction of wetting coefficients, GNPs prefer to selectively locate in the PS phase. However, when we premixed GNPs with PLA and then melt-compounded with PS, we found that a significant amount of GNPs are kinetically trapped at the interface. Thanks to the high melt viscosity of the polymer matrix and the relatively large lateral dimension of GNPs, the interfacial GNPs can remain at the interface, even after 60 min of static annealing at the processing temperature. For the (PLA/GNPs)/PS blends, although both the viscosity increase by GNPs located in the PS phase and the interfacial GNPs network formed along the interface contribute to coarsening suppression, the formation of an interfacial GNPs network plays a dominant role in the stabilization of co-continuous morphology.

To examine the influence of kinetics on the migration and localization of GNPs in the co-continuous PLA/PS blends, we have prepared blends with different melt-compounding sequences and times. We found that when GNPs were premixed with PS and then melt-compounded with PLA, all GNPs remain in the premixed PS and few interfacial GNPs could be observed under TEM. In addition, both the storage modulus and conductivity of the (PS/GNPs)/PLA_0.5 wt % blend during annealing is much smaller than that of its counterpart (PLA/GNPs)/PS_0.5 wt % blend. This further confirmed that the interfacial GNPs, rather than the GNPs located in the PS phase, lead to an increase of storage modulus and conductivity.

Finally, to systemically investigate the effect of melt-compounding times on the migration and localization of GNPs, we combined morphology, rheology, and conductivity measurements of (PLA/GNPs)/PS_0.5 wt % blends with different melt-compounding times. We showed that the static annealing does not change the amount of interfacial GNPs. The migration of interfacial GNPs to the PS phase during annealing is negligible. We also found that the formation of interfacial GNPs network facilitates increases in coarsening suppression, storage modulus, and conductivity. With the same GNPs loading, the 30 s compounded blend gives rise to a higher interfacial GNPs percentage than blends with longer compounding times (5 and 10 min). We argue that this observation is due to the synergistic effect of the encapsulation of interfacial GNPs via the folding of interfaces and the orientation-dependent migration of interfacial GNPs during melt compounding. Hence, the shorter melt-compounding time in this study contributes to more-effective coarsening suppression, larger storage moduli, and higher conductivities.

With proper control of the compounding sequences and melt-compounding times, we can kinetically locate GNPs at the interface of PLA/PS co-continuous blends and achieve a room-temperature conductivity of $\sim 10^{-6}$ S/cm, which is a value that is useful for antistatic applications. Without relying on any chemical modification of GNPs, this kinetic method, by adjusting compounding sequences and melt-compounding times to control graphene localization, could potentially have broad applications in the industrial production of conductive polymer composites.

■ ASSOCIATED CONTENT

Supporting Information

The Supporting Information is available free of charge on the ACS Publications website at DOI: 10.1021/acs.langmuir.7b03085.

Characterization of GNPs thickness and lateral dimensions, melt-compounding shear rate study, interfacial energy calculation, rheology and conductivity of PS/GNPs composites (PDF)

■ AUTHOR INFORMATION

Corresponding Authors

*E-mail: xcheng@umn.edu (X. Cheng).
*E-mail: macosko@umn.edu (C. W. Macosko).

ORCID

Xiang Cheng: 0000-0002-2759-764X

Notes

The authors declare no competing financial interest.

■ ACKNOWLEDGMENTS

The authors are grateful to Dr. Sung Cik Mun for his help in average size and thickness characterization of GNPs. The project is funded by the Joint Polymer Processing Grant by Petroleum Institute (No. 3006-11093-00036476) and U.S. National Science Foundation (No. CMMI-1661666).

■ REFERENCES

(1) Hu, K.; Kulkarni, D. D.; Choi, I.; Tsukruk, V. V. Graphene-Polymer Nanocomposites for Structural and Functional Applications. *Prog. Polym. Sci.* **2014**, *39* (11), 1934−1972.

(2) Stankovich, S.; Dikin, D. A.; Dommett, G. H. B.; Kohlhaas, K. M.; Zimney, E. J.; Stach, E. A.; Piner, R. D.; Nguyen, S. T.; Ruoff, R. S. Graphene-Based Composite Materials. *Nature* **2006**, *442* (7100), 282−286.

(3) Qi, X.-Y.; Yan, D.; Jiang, Z.; Cao, Y.-K.; Yu, Z.-Z.; Yavari, F.; Koratkar, N. Enhanced Electrical Conductivity in Polystyrene Nanocomposites at Ultra-Low Graphene Content. *ACS Appl. Mater. Interfaces* **2011**, *3*, 3130−3133.

(4) Mao, C.; Zhu, Y.; Jiang, W. Design of Electrical Conductive Composites: Tuning the Morphology to Improve the Electrical Properties of Graphene Filled Immiscible Polymer Blends. *ACS Appl. Mater. Interfaces* **2012**, *4* (10), 5281−5286.

(5) Sumita, M.; Sakata, K.; Asai, S.; Miyasaka, K.; Nakagawa, H. Dispersion of Fillers and the Electrical Conductivity of Polymer Blends Filled with Carbon Black. *Polym. Bull.* **1991**, *25*, 265−271.

(6) Tan, Y.; Fang, L.; Xiao, J.; Song, Y.; Zheng, Q. Grafting of Copolymers onto Graphene by Miniemulsion Polymerization for Conductive Polymer Composites: Improved Electrical Conductivity and Compatibility Induced by Interfacial Distribution of Graphene. *Polym. Chem.* **2013**, *4* (10), 2939.

(7) Bai, L.; He, S.; Fruehwirth, J. W.; Stein, A.; Macosko, C. W.; Cheng, X. Localizing Graphene at the Interface of Cocontinuous Polymer Blends: Morphology, Rheology, and Conductivity of Cocontinuous Conductive Polymer Composites Polymer Composites. *J. Rheol.* **2017**, *61*, 575−587.

(8) Tu, C.; Nagata, K.; Yan, S. Influence of Melt-Mixing Processing Sequence on Electrical Conductivity of Polyethylene/Polypropylene Blends Filled with Graphene. *Polym. Bull.* **2017**, *74*, 1237−1252.

(9) Gubbels, F.; Jerome, R.; Vanlathem, E.; Deltour, R.; Blacher, S.; Brouers, F. Kinetic and Thermodynamic Control of the Selective Localization of Carbon Black at the Interface of Immiscible Polymer Blends. *Chem. Mater.* **1998**, *10*, 1227−1235.

(10) Song, Y.; Xu, C.; Zheng, Q. Styrene-Butadiene-Styrene Copolymer Compatibilized Carbon Black/polypropylene/polystyrene

DOI: 10.1021/acs.langmuir.7b03085
Langmuir 2018, 34, 1073−1083

Composites with Tunable Morphology, Electrical Conduction and Rheological Stabilities. *Soft Matter* **2014**, *10* (15), 2685−2692.
(11) Chen, J.; Shi, Y.; Yang, J.; Zhang, N.; Huang, T.; Chen, C.; Wang, Y.; Zhou, Z. A Simple Strategy to Achieve Very Low Percolation Threshold via the Selective Distribution of Carbon Nanotubes at the Interface of Polymer Blends. *J. Mater. Chem.* **2012**, *22* (42), 22398−22404.
(12) Göldel, A.; Marmur, A.; Kasaliwal, G. R.; Pötschke, P.; Heinrich, G. Shape-Dependent Localization of Carbon Nanotubes and Carbon Black in an Immiscible Polymer Blend during Melt Mixing. *Macromolecules* **2011**, *44* (15), 6094−6102.
(13) Göldel, A.; Kasaliwal, G. R.; Pötschke, P.; Heinrich, G. The Kinetics of CNT Transfer between Immiscible Blend Phases during Melt Mixing. *Polymer* **2012**, *53* (2), 411−421.
(14) Shen, Y.; Zhang, T.; Yang, J.; Zhang, N.; Huang, T.; Wang, Y. Selective Localization of Reduced Graphene Oxides at the Interface of PLA/EVA Blend and Its Resultant Electrical Resistivity. *Polym. Compos.* **2017**, *38*, 1982−1991.
(15) Feng, J.; Chan, C.; Li, J. A Method To Control the Dispersion of Carbon Black in an Immiscible Polymer Blend. *Polym. Eng. Sci.* **2003**, *43* (5), 1058−1063.
(16) Liebscher, M.; Tzounis, L.; Pötschke, P.; Heinrich, G. Influence of the Viscosity Ratio in PC/SAN Blends Filled with MWCNTs on the Morphological, Electrical, and Melt Rheological Properties. *Polymer* **2013**, *54* (25), 6801−6808.
(17) Gubbels, F.; Jerome, R.; Teyssié, P.; Vanlathem, E.; Deltour, R.; Calderone, A.; Parenté, V.; Brédas, J. L. Selective Localization of Carbon Black in Immmiscible Polymer Blends: A Useful Tool to Design Electrical Conductive Composites. *Macromolecules* **1994**, *27*, 1972−1974.
(18) Cheah, K.; Forsyth, M.; Simon, G. P. Processing and Morphological Development of Carbon Black Filled Conducting Blends Using a Binary Host of Poly (Styrene Co-Acrylonitrile) and Poly (Styrene). *J. Polym. Sci., Part B: Polym. Phys.* **2000**, *38*, 3106−3119.
(19) Huang, J.; Mao, C.; Zhu, Y.; Jiang, W.; Yang, X. Control of Carbon Nanotubes at the Interface of a Co-Continuous Immiscible Polymer Blend to Fabricate Conductive Composites with Ultralow Percolation Thresholds. *Carbon* **2014**, *73*, 267−274.
(20) Taghizadeh, A.; Favis, B. D. Carbon Nanotubes in Blends of Polycaprolactone/Thermoplastic Starch. *Carbohydr. Polym.* **2013**, *98* (1), 189−198.
(21) Tan, Y.; Song, Y.; Cao, Q.; Zheng, Q. Characterization of Carbon Black-Filled Immiscible Polypropylene/polystyrene Blends. *Polym. Int.* **2011**, *60* (5), 823−832.
(22) Baudouin, A. C.; Devaux, J.; Bailly, C. Localization of Carbon Nanotubes at the Interface in Blends of Polyamide and Ethylene-Acrylate Copolymer. *Polymer* **2010**, *51* (6), 1341−1354.
(23) Bai, L.; Fruehwirth, J. W.; Cheng, X.; Macosko, C. W. Dynamics and Rheology of Nonpolar Bijels. *Soft Matter* **2015**, *11* (26), 5282−5293.
(24) Thomas, E. L.; Talmon, Y. Selective Electron Beam Etching of Multicomponent Polymer Systems. *Polymer* **1978**, *19*, 225−227.
(25) Kilbride, B. E.; Coleman, J. N.; Fraysse, J.; Fournet, P.; Cadek, M.; Drury, a.; Hutzler, S.; Roth, S.; Blau, W. J. Experimental Observation of Scaling Laws for Alternating Current and Direct Current Conductivity in Polymer-Carbon Nanotube Composite Thin Films. *J. Appl. Phys.* **2002**, *92* (7), 4024.
(26) Huang, S.; Bai, L.; Trifkovic, M.; Cheng, X.; Macosko, C. W. Controlling the Morphology of Immiscible Cocontinuous Polymer Blends via Silica Nanoparticles Jammed at the Interface. *Macromolecules* **2016**, *49* (10), 3911−3918.
(27) Owens, D. K.; Wendt, R. C. Estimation of the Surface Free Energy of Polymers. *J. Appl. Polym. Sci.* **1969**, *13* (8), 1741−1747.
(28) Owens, D. K. Some Thermodynamic Aspects of Polymer Adhesion. *J. Appl. Polym. Sci.* **1970**, *14* (7), 1725−1730.
(29) Liu, X.-Q.; Li, R.-H.; Bao, R.-Y.; Jiang, W.-R.; Yang, W.; Xie, B.-H.; Yang, M.-B. Suppression of Phase Coarsening in Immiscible, Cocontinuous Polymer Blends under High Temperature Quiescent Annealing. *Soft Matter* **2014**, *10*, 3587−3596.
(30) Zaikin, A. E.; Karimov, R. R.; Arkhireev, V. P. A Study of the Redistribution Conditions of Carbon Black Particles from the Bulk to the Interface in Heterogeneous Polymer Blends. *Colloid J.* **2001**, *63* (1), 53−59.
(31) Jalali Dil, E.; Favis, B. D. Localization of Micro- and Nano-Silica Particles in Heterophase Poly (Lactic Acid)/ Poly (Butylene Adipate-Co-Terephthalate) Blends. *Polymer* **2015**, *76*, 295−306.
(32) Blake, T. D.; De Coninck, J. The Influence of Solid-Liquid Interactions on Dynamic Wetting. *Adv. Colloid Interface Sci.* **2002**, *96*, 21−36.
(33) Blake, T. D. The Physics of Moving Wetting Lines. *J. Colloid Interface Sci.* **2006**, *299*, 1−13.
(34) Plattier, J.; Benyahia, L.; Dorget, M.; Niepceron, F.; Tassin, J.-F. Viscosity-Induced Filler Localisation in Immiscible Polymer Blends. *Polymer* **2015**, *59*, 260−269.

DOI: 10.1021/acs.langmuir.7b03085
Langmuir 2018, 34, 1073−1083